# Connected-Slot Array with Artificial Dielectrics
## A 6 to 15 GHz Dual-Pol Wide-Scan Prototype

Cavallo, Daniele; Syed, Waqas H.; Neto, Andrea

**DOI**
10.1109/TAP.2018.2811841

**Publication date**
2018

**Document Version**
Accepted author manuscript

**Published in**
IEEE Transactions on Antennas and Propagation

# Communication

## Connected-Slot Array with Artificial Dielectrics: A 6 to 15 GHz Dual-Pol Wide-Scan Prototype

Daniele Cavallo, Waqas H. Syed, and Andrea Neto

***Abstract*— In this work we report on the design, manufacturing and testing of a dual-polarized array of connected slots radiating in the presence of an artificial dielectric superstrate. The prototype array consists of 512 elements, i.e. 16×16 connected slots for each of the two polarizations. The antenna array is realized with a single multi-layer printed circuit board (PCB), which represents an advantage in terms of cost and complexity with respect to the typical configuration based on multiple vertically arranged PCBs. The performance is investigated in terms of simulated and measured matching characteristics and radiation patterns. The proposed structure achieves active voltage standing wave ratio (VSWR) lower than 3.1 over about an octave bandwidth (6 to 15 GHz), within a wide scan range (±60° in the $H$-plane and ±80° in the $E$-plane).**

***Index Terms*— Artificial dielectric, connected arrays, wideband arrays, wide-scan array.**

### I. Introduction

THERE has been a growing interest, in the last decade, in the development of phased arrays that can operate over wide bandwidths and wide scan ranges. Such characteristics are desired to support multifunction operation for both communication and radar applications and to reduce the number of antennas on complex platforms, where there is limited space available to accommodate an ever increasing number of sensors. To include communication services, these arrays should also provide polarization agility, to allow variable settings of radiation and higher information capacity.

Several solutions have been proposed to realize wideband wide-scanning arrays. These include stacked patches [1], tapered slot antennas [2]–[4], metal flared-notch elements [5], [6], long-slot arrays [7], [8] and tightly-coupled dipole arrays [9]–[12]. These examples have attained wideband properties, with bandwidths spanning from 40% to over a decade, but typically broader matching bandwidths are achieved at the cost of increased cross-polarization (X-pol) levels, reduced scan range or decreased total efficiency. Moreover, most of the above mentioned designs are based on array configurations where the radiating elements and the feed structure are printed on vertical printed circuit boards (PCBs) [13]. This arrangement can lead to costly assembly whose complexity increases when scaling down the array dimensions to operate at higher frequency.

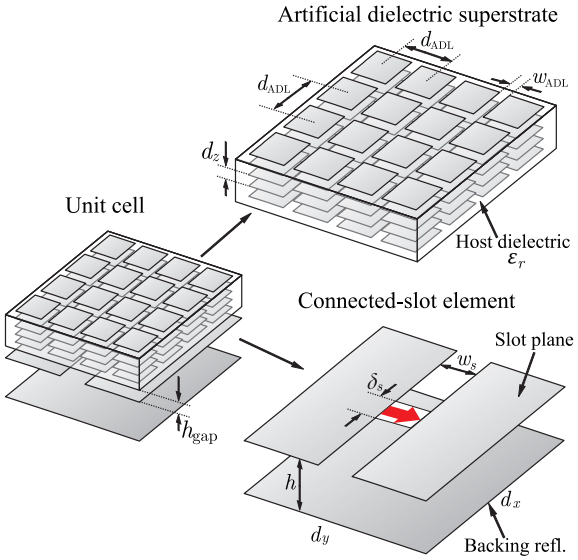


Fig. 1. Unit cell of a connected array of slots in the presence of a backing reflector and loaded with ADLs.

In this work, the goal is to implement the array with a single multi-layer planar structure, targeting a frequency range that includes the Ku-band, which is commonly utilized for different communication services. This configuration would be low-cost and easier to manufacture, compared to the vertical arrangement of the antenna PCBs. A planar solution for wideband phased array was presented in [14], where a 3:1 planar design was shown to scan up to 45° in all azimuth planes, maintaining efficiency above 80%. Another planar design was shown in [15] for a narrower bandwidth 8-12.5 GHz, but wider scanning up to 60° and 75° on the $H$- and $E$-plane, respectively. However, in this last design, the feed is not realized with plated-through holes but by inserting metal pins in a foam substrate, which is a non-standard PCB manufacturing process.

Recently, we presented an alternative concept that allows for a completely planar implementation [16]. This consists of an array of connected slots with artificial dielectric layers (ADLs) as a superstrate, with a 6-to-15 GHz bandwidth. The artificial dielectric is used in place of a real dielectric because of its anisotropy, [18] which is a key property to avoid the excitation of surface waves and the occurrence of scan blindness. The ADLs also perform a wideband impedance transformation, as

Manuscript received Month DD, YYYY; revised Month DD, YYYY; accepted Month DD, YYYY. Date of publication Month DD, YYYY; date of current version Month DD, YYYY. This work was supported by the European Research Council starting grant ERC-2011-StG AAATSI no. 278794, by the Dutch technology foundation (STW) under project code 10709, and by the Netherlands Organization for Scientific Research (NWO) VENI Grant no. 13673. *(Corresponding author: Daniele Cavallo)*

The authors are with the Microelectronics Department, Delft University of Technology, 2628 CD Delft, The Netherlands (e-mail: d.cavallo@tudelft.nl).

Color versions of one or more of the figures in this communication are available online at http://ieeexplore.ieee.org.

Digital Object Identifier XX.XXXX/TAP.XXXX.XXXXXXXX.

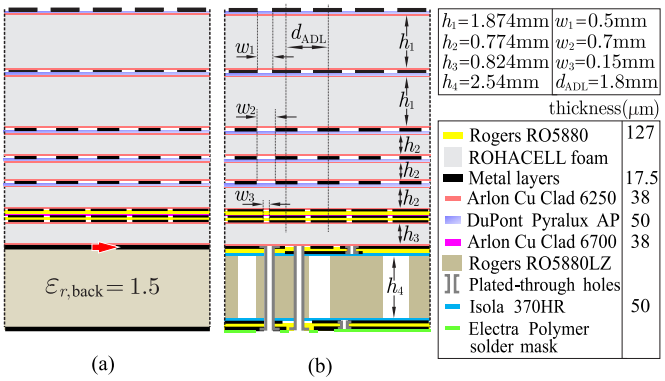


Fig. 2. Stackup of (a) the simplified array unit cell and (b) the detailed array unit cell, including the integrated feeding network, the vias and the perforated dielectric substrate.

proposed in [17]. Figure 1 shows the idealized array unit cell including the connected slot element and the ADLs, which are layers of periodic, electrically small, metal patches included in a dielectric host medium to synthesize a higher equivalent refractive index [19]. When the array is loaded with a single or multiple ADL slabs, the radiation from the slots is mainly directed upward, thus the distance from the ground plane $h$ can be greatly reduced without strongly degrading the impedance matching properties. This lower distance enables the realization of the feeding lines by means of standard via-hole technology, e.g. for X- or Ku-band designs. Consequently, a fully planar implementation of the array is enabled.

In this article, we report on the development of a prototype based on the concept introduced in [16]. Following up on that work, the design presented here is improved on a number of aspects: the array in [16] was single polarized and scanning up to 50° and its performance was only characterized in terms of infinite array simulations; here the goal is to extend the design from single-pol to dual-pol operation and to further increase the scan range to 60° or above. Furthermore, we present the first experimental validation of this antenna concept and report on the measured performance.

## II. Antenna Element Design

By following the same procedure as [16], we first design a unit cell as shown in Fig. 2(a), employing analytical models that allow the prediction of the active impedance, in an infinite array environment, with negligible computational costs. The ADL slab includes 8 layers, whose geometrical parameters are optimized to implement a wideband transformation from the free-space impedance to 65 Ω at the input port on the slot, while maximizing the scan range. The bonding layers to be used in the real ADL stackup are taken into account in the analytical tool already from the early design phase, since they can significantly influence the ADL properties. The unit cell in Fig. 2(a) is still idealized because it considers a single, linearly polarized, slot fed with a delta-gap excitation (as in the inset of Fig. 1) and a homogeneous substrate with low relative permittivity ($\varepsilon_{r,\text{back}} = 1.5$) between the slot plane and the backing reflector.

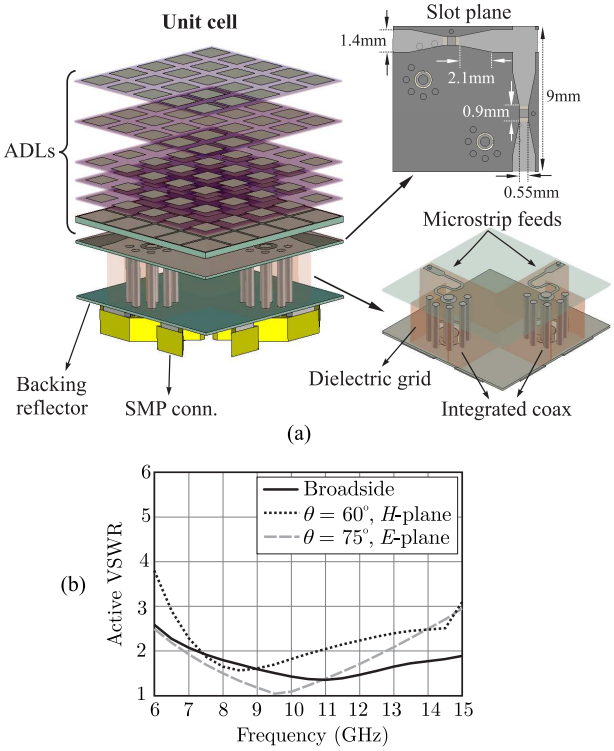


Fig. 3. (a) Three-dimensional view of the final unit cell and (b) active VSWR for broadside and scanning to 60° in the $H$-plane and to 75° in the $E$-plane.

The optimized unit cell in Fig. 2(a) is subsequently modified to include two orthogonal slots for the dual-polarized operation, and to incorporate a realistic feed realized with microstrips and integrated coaxial lines. Moreover, a perforated dielectric is employed to realize the material with low permittivity ($\varepsilon_{r,\text{back}} = 1.5$). The final unit cell stackup is shown in Fig. 2(b), with the choice of the used materials and the dimensions.

The three-dimensional view of the unit cell with the details of the feeding structure is shown in Fig. 3(a). This detailed unit cell has been simulated with CST [20] and the resulting active voltage standing wave ratio (VSWR) is shown in Fig. 3(b) for broadside and scanning to 60° in the $H$-plane and to 75° in the $E$-plane. The active VSWR is lower than 3 over about an octave bandwidth, from 6.5 to 15 GHz. The scanning performance is better on the $E$-plane because, as highlighted in the dispersion analysis of ADL slabs [21], ADLs do not support transverse magnetic (TM) surface waves that limit the scanning on the $E$-plane. However, the ADL can support transverse electric (TE) surface waves, that degrade the performance at high frequency for extreme scan angle above 60°. The period of the unit cell is $d_x = d_y = 9$ mm, which corresponds to about $0.45\lambda$, where $\lambda$ is the wavelength at the highest frequency of operation 15GHz. The overall height of the layer stack is about 11 mm, which corresponds to $0.55\lambda$.

### A. Simulated X-pol Level

The simulated X-pol level is shown in Fig. 4(a) for the two diagonal planes $\phi = 45°$ and $\phi = -45°$, according to the

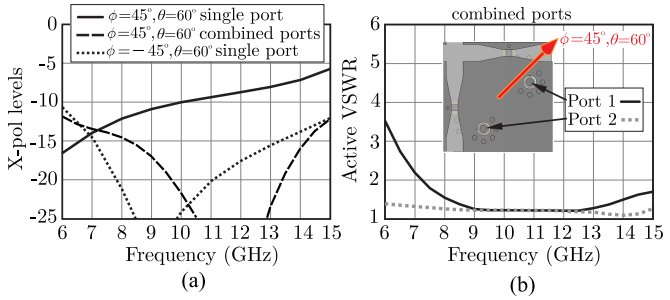


Fig. 4. (a) X-pol levels for scanning in the diagonal planes to $\theta = 60°$: $\phi = 45°$ with single port excitation (continuous line), $\phi = 45°$ with the two ports excited with proper weights to cancel the X-pol at 12 GHz (dashed line) and $\phi = -45°$ (dotted line); (b) active VSWR for the two ports when combined to cancel the X-pol for $\phi = 45°$ and $\theta = 60°$.

third Ludwig's definition [22]. It can be observed that the X-pol radiation is not the same in the two diagonal planes, due two the asymmetry of the feed and the dielectric grid used for the substrate. In the worst case, the X-pol is about $-6.5$ dB at the highest frequency of operation. These levels of X-pol are in line with what is expected from planar arrays in the presence of dielectric superstrates. It is known that the X-pol of linearly polarized sources might increase due to the presence of dielectric slabs [23] and artificial dielectrics are not an exception.

However, it is possible to combine the two orthogonal ports in such a way to perfectly cancel the X-pol at a certain frequency for a specific angle. For example, the dashed curve in Fig. 4(a) shows such cancellation done at 12 GHz, for scanning to 60° in the diagonal plane ($\phi = 45°$). It can be noted that the compensation is wideband, as the X-pol level is reduced to below $-12$ dB over the entire target bandwidth. On the contrary, a similar compensation is very narrow-band when attempting to cancel the X-pol caused by common-mode resonances in arrays of tightly-coupled dipoles or Vivaldi antennas [24]. Moreover, when combining the ports to cancel the X-pol, the matching remains good, as shown in Fig. 4(b).

## III. Investigation on the Edge Effects

In connected arrays, it is especially important to assess the finite edge effects [25], [26]. To demonstrate the effect of the finiteness, we simulate infinite-by-finite arrays using the semi-analytical tool presented in [16]. Maps of the active VSWR as a function of the frequency and the element index are presented in Fig. 5. The array is assumed to be finite in the plane in which the elements are connected ($H$-plane), where typically the edge effects are more severe [26], and to be scanning to 60° in the same plane. Figure 5(a) refers to the case in which all the elements of a $16\times\infty$ array are uniformly fed. It can be seen that some of the elements, even the ones close to center, exhibit high values of VSWR ($\approx 4$). The simulated VSWR of the same array fed with a raised cosine amplitude taper is presented in Fig. 5(b) and exhibits improved matching properties for the elements in the center of the array, while strong mismatch occurs for the elements close to the edge that are weighted by lower amplitudes. The

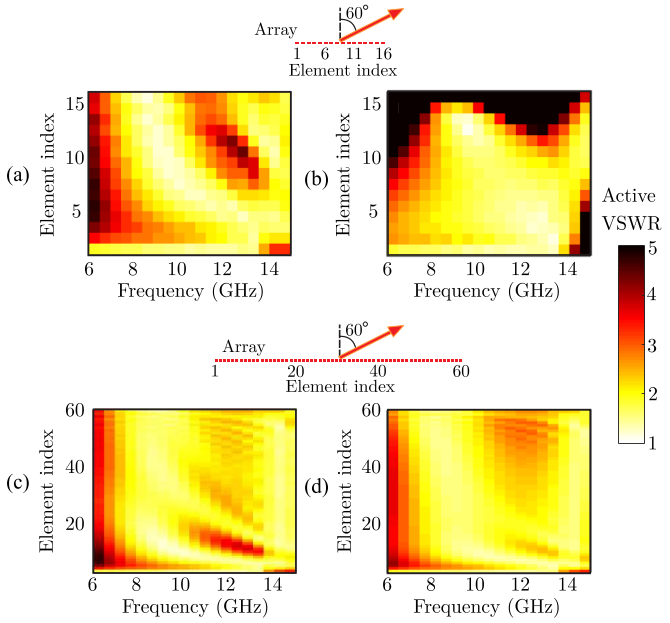


Fig. 5. Active VSWR as a function of frequency and element index: (a), (b) $16\times\infty$ elements without and with amplitude taper, respectively; (c), (d) $60\times\infty$ elements without and with amplitude taper, respectively; scanning to 60° in the $H$-plane is considered.

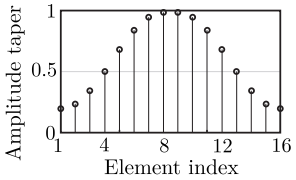


Fig. 6. Amplitude taper.

considered taper is shown in Fig. 6. It can be also pointed out that an array of 16 elements is still rather small, while an operative system for Satcom or radar applications would likely consists of a much larger number of elements. To assess the properties of larger arrays, Figs. 5(c) and (d) reports the active VSWR for $60\times\infty$ elements scanning to 60° in the $H$-plane, without and with tapering, respectively. It is evident that larger radiating apertures suffer less from edge effects and mismatch issues, especially when illumination taper is applied.

## IV. Array Prototype

Based on the design described in Sec. II, a prototype array has been manufactured, consisting of 512 elements, i.e. $16\times16$ connected slots for each polarization. The photos of the demonstrator are shown in Fig. 7. More specifically, Fig. 7(a) displays the antenna board with connected slots before it is assembled with the ADL slab, whereas Fig. 7(b) represents a view of the entire array with the ADLs and the antenna bonded together. The slots at the array edges are extended by about $4 \sim 5$cm, so that power propagating attenuates by radiation and undergoes reduced reflection at the termination.

In this section the measured results of the demonstrator are presented, including the matching characteristics of a central element and the radiation patterns of the entire array.

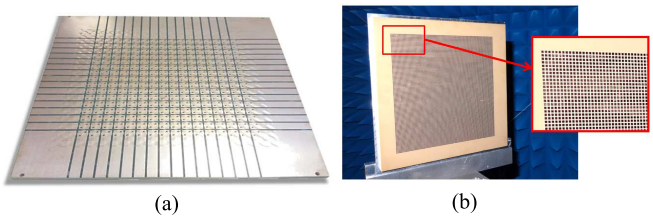


Fig. 7. Photo of the array prototype: (a) connected array of slots and (b) same array with ADL superstrate.

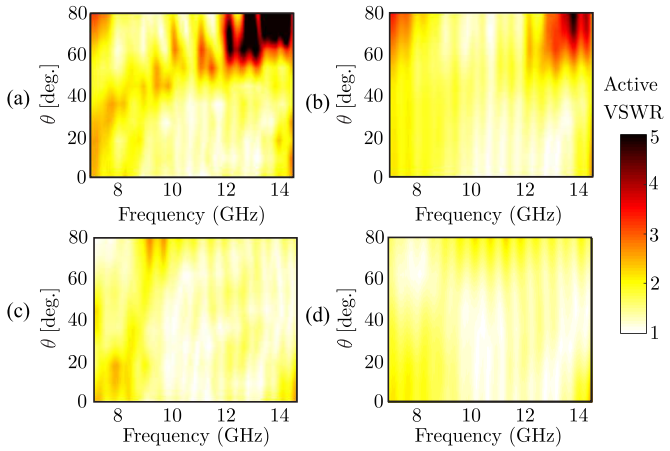


Fig. 8. Measured active VSWR of a central element of the array as a function of frequency and scanning angle in the (a) $H$-plane without amplitude taper, (b) $H$-plane with amplitude taper, (c) $E$-plane without amplitude taper, (b) $E$-plane with amplitude taper.

### A. Measured Matching Properties of a Central Element

The measured active (VSWR) of a central element of the array is shown in Fig. 8, as a function of the frequency and of the scanning angle. Given the high number of elements, the coupling parameters were measured for one quadrant of the array ($8 \times 8$ S-parameters for each polarization) and assumed to be symmetric for the remaining quadrants.

Figures 8(a) and (b) refer to the case of scanning in the $H$-plane, without and with amplitude taper, respectively, whereas Fig. 8(c) and (d) are relative to $E$-plane scanning, without and with amplitude taper, respectively. The Active VSWR for scanning in the $H$-plane remains below 2.5 over a wide scan range and starts to degrade at around $60°$ scanning, for frequency between 12 and 14 GHz. Improved matching is observed when considering a tapered illumination of the array, as it can be seen from Fig. 8(b). Better performance is obtained for scanning in the $E$-plane, for which active VSWR lower than 2.4 is measured for scanning up to $80°$, when tapering is applied.

To better visualize the VSWR levels, a few curves for specific scanning angles are presented in Fig. 9, considering amplitude taper. The VSWR is lower than 2.6 from 6 to 14.5 GHz, scanning up to $40°$ in the $H$-plane and to $80°$ in the $E$-plane. The VSWR increases to 3.1 for $60°$ scan in the $H$-plane. These results are in fair agreement with the performance predicted by the infinite array simulations in Fig. 3(b). The differences between the measured and the

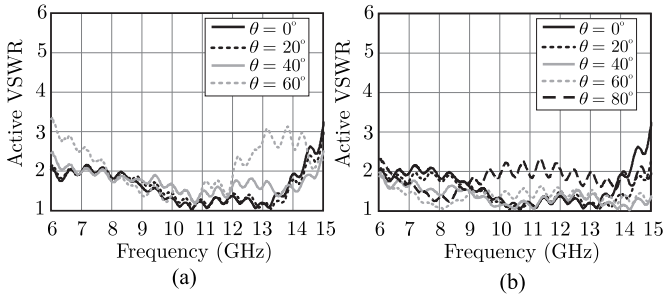


Fig. 9. Measured active VSWR of a central element of the array in the (a) $H$- and (b) $E$-plane for different scanning angles and in the presence of amplitude taper.

infinite array simulation are mainly due to edge effects arising from the truncation of the array. However, we showed from simulations in Fig. 7 that better matching performance can be expected from larger radiating apertures.

### B. Measured Active Element Pattern

The active element pattern of central element of the array has been measured on the main planes and the two diagonal planes. Figure 10 shows a number of cuts of the active element pattern, at the two frequencies of 8 and 13 GHz. Fluctuations of a few dB can be noted in the co-polar patterns, which are mainly due to reflection from the metal frame around the array. It can be observed that the X-pol levels are lower than $-15$ dB for the entire scan range in the main planes and in one of the diagonal planes ($\phi = -45°$). However, higher X-pol levels are obtained in the other diagonal plane ($\phi = 45°$), especially at the higher frequency. Such result is consistent with what observed from simulations (Fig. 4). The active element pattern is wider in beamwidth in the $E$-plane (Fig. 10(a)) as compared to the $H$-plane pattern. This is a consequence of the better matching performance of the array when scanning in the $E$-plane to wide angles.

The active broadside gain of the central element has also been measured and is presented in Fig. 11. The gain is multiplied by the number of elements, to give an idea of the total array gain, if all the elements behaved like the central one. The array gain from a $16\times16$ array simulated with CST, under infinite array approximation, is also shown. This corresponds to the maximum theoretical directivity that can be achieved from an aperture equal to the area of $16\times16$ unit cells. Since the ADL superstrate is larger than the slot array and effectively increases the aperture size, the gain exceeds the theoretical curve in most of the operational frequency band. The directivity limit is computed also using the total area including the extended artificial dielectric structure, to match better the obtained gain levels.

Moreover, an array of $16\times16$ is still not large enough to be accurately described by the infinite array approximation. Therefore, measured patterns of the entire array are needed to further assess the radiation characteristics.

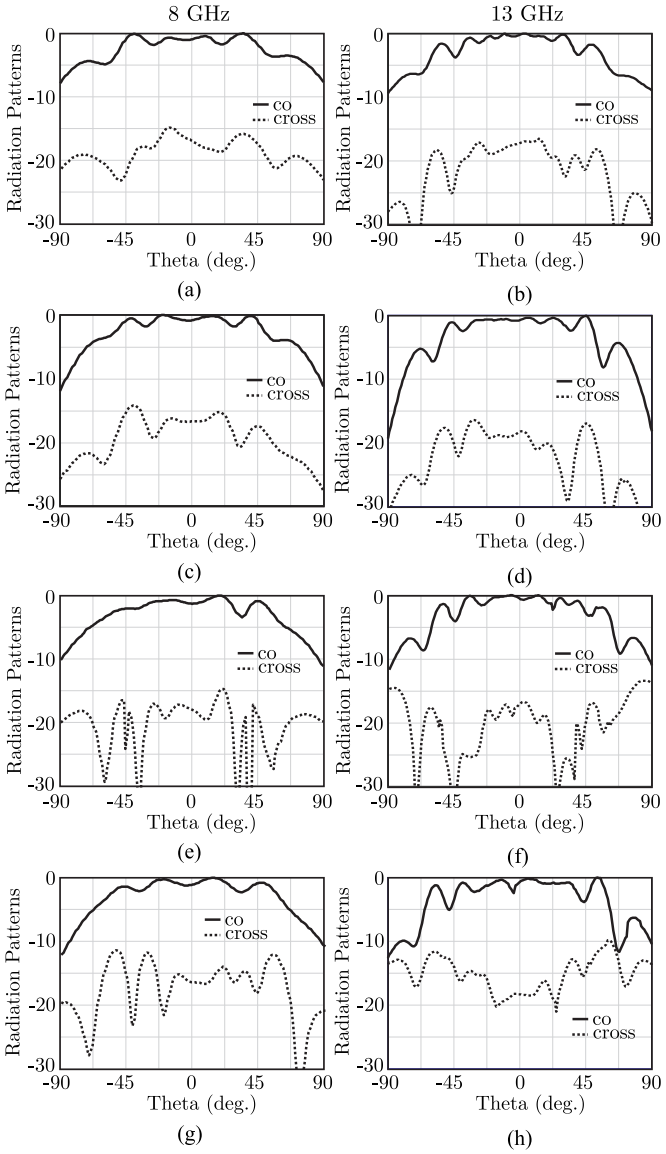


Fig. 10. Measured normalized co-pol and X-pol active element patterns of a central element of the array at 8 GHz and 13 GHz: (a), (b) $E$-plane; (c), (d) $H$-plane; (e), (f) $D$-plane $\phi = -45°$; (g), (h) $D$-plane $\phi = 45°$.

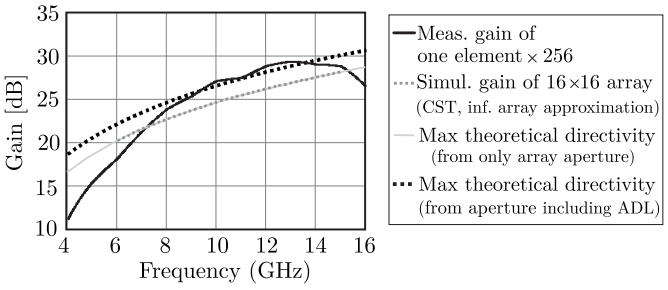


Fig. 11. Array broadside gain assuming all elements are described by the measured gain of the central element, compared with the simulated gain with CST under infinite array approximation. The theoretical maximum directivity for the aperture is also plotted, using both the area of only the active slots, as well as the larger area including the extended artificial dielectric structure.

### C. Measured Radiation Patterns with Existing Beam Former

To measure the radiation patterns of the entire array, the prototype has been tested in combination with a beamforming system previously developed in [12]. Uniform amplitude illumination of the array element is considered. The measured co-polar and cross-polar radiation patterns for scanning to 0°, 30° and 60° in the $H$- and $E$-planes are shown in Fig. 12, for three frequencies (8.4, 11 and 14.5 GHz). The patterns are normalized to the maximum power measured at broadside scanning, thus the variation of gain with scanning can be determined from the figures. A 2 to 3 dB drop for scanning to 60° can be observed for the co-polar component, with respect to the broadside value. The X-pol ratio is also below −13 dB for all considered scanning conditions on the main planes.

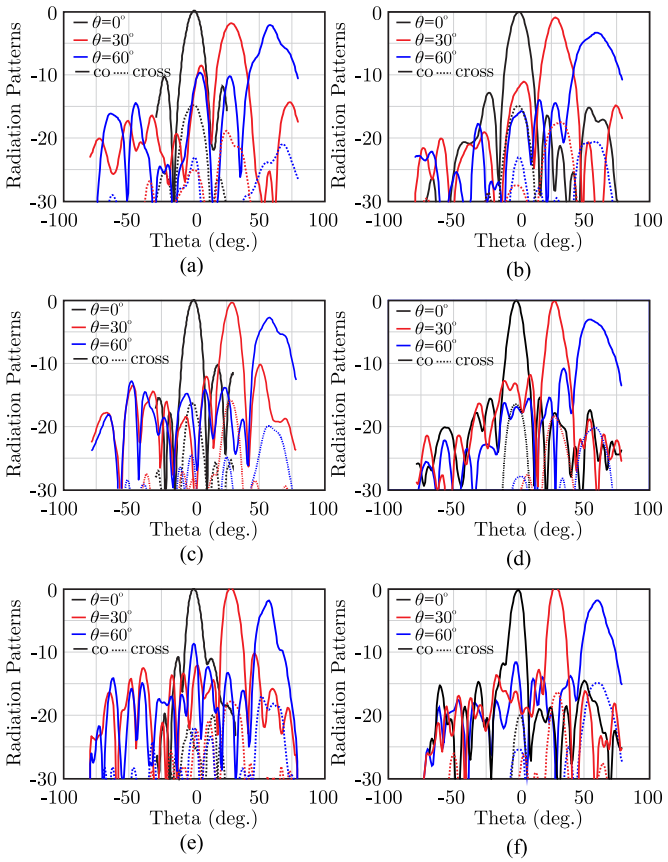


Fig. 12. Measured co-polar and cross-polar radiation patterns for scanning to 0°, 30° and 60°: (a) $H$- and (b) $E$-planes at 8.4 GHz, (c) $H$- and (d) $E$-planes at 11 GHz, (e) $H$- and (f) $E$-planes at 14.5 GHz.

The measured co-polar and cross-polar radiation patterns for scanning to 60 degrees in the two diagonal planes are presented in Fig. 13. As it was predicted from simulations, the X-pol level is higher for one of the two diagonal planes, an reaches −5.5 dB at 14.5 GHz for scanning to $\theta = 60°$ and $\phi = 45°$. This value is 1 dB higher than the one calculated with infinite array simulations.

The measured gain of the array when fed by the beamforming system is not provided because of the large uncertainty related to the beamformer itself: an accurate characterization of the S-parameters of the beamformer for all different settings of amplitude and phase was not available, especially when loaded by the array; moreover, amplitude and phase calibration at each output channel of the beamformer was not applied.

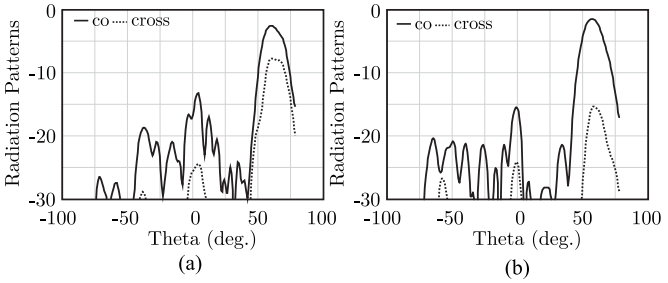


Fig. 13. Measured co-polar and cross-polar radiation patterns for scanning to 60 degrees in the $D$-plane: (a) $\phi = 45°$, $\theta = 60°$ (b) $\phi = -45°$, $\theta = 60°$ .

## V. Conclusions

We presented a dual-polarized array prototype operating from 6 to 15 GHz, based on connected arrays of slots radiating in the presence of artificial dielectric superstrates. The array includes 512 elements, i.e. 16×16 for each polarization. The proposed concept is cost effective, since it is realized by a single printed circuit board with multiple layers and does not require complex assembly. The array was tested and the measured matching and radiation characteristics were presented.

The artificial dielectric slab, because of its anisotropy, allows to shift the onset of surface waves to higher frequencies compared to a real dielectric slab, thus enabling wider scan ranges. Experimental results showed scanning capability up to $60°$ in all azimuth planes with scan loss (compared to the broadside maximum gain) better than 3 dB.

The measured active VSWR for a central element was also reported to be lower than 2.6 from 6 to 14.5 GHz, scanning up to $40°$ in the $H$-plane and to $80°$ in the $E$-plane. The VSWR increases to 3.1 for $60°$ scan in the $H$-plane. The edge effects were investigated by means of full-wave simulations and were shown to be a likely cause for the observed differences between infinite array simulations and measurements. Larger arrays are expected to have higher matching efficiency from simulation-based predictions.

Measured X-pol levels are below $-13$ dB for the main planes and they reach $-5.5$ dB in the worst case for diagonal plane. We showed nonetheless how an opportune combination of the two ports with proper weights can be used to cancel lower the X-pol levels over the entire bandwidth of operation.

## Acknowledgements

The authors would like to thank Pascal Aubry for the support in the measurements and Michiel Bruin, Frans Nennie, Rob Boekema, and Roland Bolt from TNO, for the help with the assembly and the testing of the radiation characteristics.

## References

[1] L. Infante, S. Mosca and M. Teglia, "Low-profile wide-band wide-angle-scan antenna array element," in *Proc. Eur. Conf. Antennas Propag.*, Prague, Czeck Republic, Mar. 2012, pp. 638-642.

[2] D. H. Schaubert, S. Kasturi, A. O. Boryssenko, and W. M. Elsallal, "Vivaldi antenna arrays for wide bandwidth and electronic scanning," in *Proc. Eur. Conf. Antennas Propag.*, Edinburgh, U.K., Nov. 2007, pp. 1-6.

[3] J. J. Lee, S. Livingston and R. Koenig, "A low-profile wide-band (5:1) dual-pol array," *IEEE Antennas Wireless Propag. Lett.*, vol. 2, no. 1, pp. 46-49, 2003.

[4] W. Elsallal, J. B. West, J. Wolf, R. Freeman, R. Legge, V. Olen, T. W. Darymple, M. B. Longbrake, and P. E. Buxa, "Charateristics of decade-bandwidth, Balanced Antipodal Vivaldi Antenna (BAVA) phased arrays with time-delay beamformer systems," *IEEE Int. Symp. Phased Array Systems & Technology*, Waltham, MA, USA, Oct. 2013, pp. 111-116.

[5] H. Holter, "Dual-polarized broadband array antenna with BOR elements, mechanical design and measurements," *IEEE Trans. Antennas Propag.*, vol. 55, no. 2, pp. 305-312, Feb. 2007.

[6] R. W. Kindt, W. R. Pickles, "Ultrawideband all-metal flared-notch array radiator," *IEEE Trans. Antennas Propag.*, vol. 58, no. 11, pp. 3568-3575, Sep. 2010.

[7] J. J. Lee, S. Livingston, R. Koenig, D. Nagata, and L. L. Lai, "Compact light weight UHF arrays using long slot apertures," *IEEE Trans. Antennas Propag.*, vol. 54, no. 7, pp. 2009-2015, Jul. 2006.

[8] J. J. Lee, S. Livingston, and D. Nagata, "A low profile 10:1 (2002000 MHz) wide band long slot array," in *Proc. IEEE Antennas Propag. Soc. Int. Symp.*, San Diego, CA, USA, Jul. 511, 2008, pp. 1-4.

[9] J. P. Doane, K. Sertel, and J. L. Volakis, "A wideband, wide scanning tightly coupled dipole array with integrated balun (TCDA-IB)," *IEEE Trans. Antennas Propag.*, vol. 61, no. 9, pp. 4538-4548, Sep. 2013.

[10] W. F. Moulder, K.Sertel and J. L. Volakis, "Ultrawideband superstrate enhanced substrate loaded array with integrated feed," *IEEE Trans. Antennas Propag.*, vol. 61, no. 11, pp. 5802-5807, Aug. 2013.

[11] M. H. Novak and J. L. Volakis, "Ultrawideband antennas for multiband satellite communications at UHF-Ku frequencies," *IEEE Trans. Antennas Propag.*, vol. 63, no. 4, pp. 1334-1341, Apr. 2015.

[12] R. J. Bolt, D. Cavallo, G. Gerini, D. Deurloo, R. Grooters, A. Neto, and G.Toso, "Characterization of a dual-polarized connected-dipole array for Ku-band mobile terminals," *IEEE Trans. Antennas Propag.*, vol. 64, no. 2, pp. 391-398, Feb. 2016.

[13] D. Cavallo, A. Neto, G. Gerini, A. Micco, and V. Galdi, "A 3 to 5 GHz wideband array of connected dipoles with low cross polarization and wide-scan capability," *IEEE Trans. Antennas Propag.*, vol. 61, no. 3, pp. 1148-1154, Mar. 2013.

[14] S. S. Holland, D. H. Schaubert, and M. N. Vouvakis, "A 7-21 GHz dual-polarized planar ultrawideband modular antenna (PUMA) array," *IEEE Trans. Antennas Propag.*, vol. 60, no. 10, pp. 4589-4600, Oct. 2012.

[15] J. A. Kasemodel, C.C. Chen and J. L. Volakis, "Wideband planar array with integrated feed and matching network for wide-angle scanning," *IEEE Trans. Antennas Propag.*, vol. 61, no. 9, pp. 4528-4537, Sep. 2011.

[16] W. H. Syed, D. Cavallo, H. Thippur Shivamurthy, and A. Neto, "Wide-band, wide-scan planar array of connected slots loaded with artificial dielectric superstrates," *IEEE Trans. Antennas Propag.*, vol. 64, no. 2, pp. 543-553, Feb. 2016.

[17] T. G. Waterman, "Wideband wide scan antenna matching structure using electrically floating plates," U.S. Patent 8253641 B1, Aug. 28, 2012.

[18] D. Cavallo and C. Felita, "Analytical formulas for artificial dielectrics with non-aligned layers," *IEEE Trans. Antennas Propag.*, vol. 65, no. 10, pp. 5303-5311, Oct. 2017.

[19] W. E. Kock, "Metallic delay lenses," *Bell Syst. Tech. J.*, vol. 27, no. 1, pp. 5882, Jan. 1948.

[20] *CST Microwave Studio* 2014 [Online]. Available: http://www.cst.com

[21] D. Cavallo, W. H. Syed, and A. Neto, "Closed-form analysis of artificial dielectric layers-Part II: Extension to multiple layers and arbitrary illumination," *IEEE Trans. Antennas Propag.*, vol. 62, no. 12, pp. 6265-6273, Dec. 2014.

[22] A. Ludwig, "The definition of cross polarization," *IEEE Trans. Antennas Propag.*, vol. 21, no. 1, pp. 116119, Jan. 1973.

[23] A. Hoorfar, K. C. Gupta and D. C. Chang, "Cross-polarization level in radiation from a microstrip dipole antenna," *IEEE Trans. Antennas Propag.*, vol. 36, no. 9, pp. 1197-1203, Sep 1988.

[24] R. W. Kindt and D. Taylor, "Polarization correction in dual-polarized phased arrays of flared notches," in *Proc. IEEE Antennas Propag. Soc. Int. Symp.*, July 2011.

[25] A. Neto, D. Cavallo, and G. Gerini, "Edge-born waves in connected arrays: A finite × infinite analytical representation," *IEEE Trans. Antennas Propag.*, vol. 59, no. 10, pp. 3646-3657, Oct. 2011.

[26] D. Cavallo, W. H. Syed, and A. Neto, "Equivalent transmission line models for the analysis of edge effects in finite connected and tightly-coupled arrays," *IEEE Trans. Antennas Propag.*, vol. 65, no. 4, pp. 1788-1796, Apr. 2017.